

01 Aug 1995

## A Comparison of FDTD Algorithms for Subcellular Modeling of Slots in Shielding Enclosures

Kuang-Ping Ma

James L. Drewniak

Missouri University of Science and Technology, drewniak@mst.edu

Follow this and additional works at: [https://scholarsmine.mst.edu/ele\\_comeng\\_facwork](https://scholarsmine.mst.edu/ele_comeng_facwork)



Part of the [Electrical and Computer Engineering Commons](#)

---

### Recommended Citation

K. Ma and J. L. Drewniak, "A Comparison of FDTD Algorithms for Subcellular Modeling of Slots in Shielding Enclosures," *Proceedings of the IEEE International Symposium on Electromagnetic Compatibility (1995, Atlanta, GA)*, pp. 157-162, Institute of Electrical and Electronics Engineers (IEEE), Aug 1995.

The definitive version is available at <https://doi.org/10.1109/ISEMC.1995.523538>

This Article - Conference proceedings is brought to you for free and open access by Scholars' Mine. It has been accepted for inclusion in Electrical and Computer Engineering Faculty Research & Creative Works by an authorized administrator of Scholars' Mine. This work is protected by U. S. Copyright Law. Unauthorized use including reproduction for redistribution requires the permission of the copyright holder. For more information, please contact [scholarsmine@mst.edu](mailto:scholarsmine@mst.edu).

# A Comparison of FDTD Algorithms for Subcellular Modeling of Slots in Shielding Enclosures

Kuang-Ping Ma and James L. Drewniak  
 Electromagnetic Compatibility Laboratory  
 Department of Electrical Engineering  
 University of Missouri-Rolla  
 Rolla, Missouri, 65401

## Abstract

Thin slot modeling for the Finite-Difference Time-Domain (FDTD) method is investigated. Two subcellular algorithms for modeling thin slots with the FDTD method are compared for application to shielding enclosures in EMC. The stability of the algorithms is investigated, and comparisons between the two methods for slots in planes, and slots in loaded cavities are also made.

## 1 Introduction

As the speed of the electronic designs increases, radiation from slots and seams in conducting enclosures is of greater concern. The integrity of typical shielding enclosure designs is compromised by numerous slots and apertures for CD-ROMs, heat vents, and I/O cables among others. The energy is coupled through these slots, and radiated to the external environment. Thus understanding radiation from slots, and energy coupling between slots as well as from slots to cables is very important in EMC problems.

The finite-difference time-domain (FDTD) method has been widely applied in solving many types of electromagnetic scattering problems. It possesses the advantage of simple implementation for relatively complex problems, and high accuracy. A disadvantage of the FDTD method is that significant computational resources are expended for modeling an electrically small object without the aid of special subcellular algorithms. Radiation from thin slots in enclosures as well as coupling energy from external fields to the enclosures through a thin slot fall into this category. In addition to the increased memory requirement to fully discretize a thin slot, the running time is also increased by virtue of a smaller time-step to satisfy the CFL stability criterion. Several subcellular Thin-Slot Algorithms (TSF) have been proposed to circumvent the need for fully gridding a thin slot [1] [2]. Utilizing these TSFs, a thin slot segment can be modeled with a single cell, thereby saving computational resources while retaining high accuracy. In this paper, subcellular FDTD thin-slot algorithms for simulations are considered. Two subcellular TSF algorithms developed by Gilbert and Holland [1] and Riley and Turner [2], are briefly summarized, comparison results between these two TSFs for plane-wave scattering from 3D finite plates, loaded cavities, and infinite planes are presented. Stability considerations for these two TSFs are also discussed.

## 2 FDTD Modeling

For a source free, isotropic, homogeneous, and lossless medium, Maxwell's two curl equations are given by

$$\nabla \times \vec{E} = -\mu \frac{\partial \vec{H}}{\partial t} \quad (1)$$

$$\nabla \times \vec{H} = \epsilon \frac{\partial \vec{E}}{\partial t}, \quad (2)$$

where  $\vec{E}$  and  $\vec{H}$  are the electric field and magnetic field, and  $\epsilon, \mu$  are permittivity and permeability, respectively. In rectangular coordinates, the vector curl equations can be written as six scalar equations, and a finite-difference form of the curl equations obtained using central differencing in both time and space. For example, the finite-difference equation for the  $\hat{z}$ -component of the electric field is

$$\begin{aligned} E_{z,i,j,h}^{n+1} &= E_{z,i,j,h}^n + \frac{\Delta t}{\epsilon \Delta x} (H_{y,i+1,j,h}^{n+\frac{1}{2}} - H_{y,i,j,h}^{n+\frac{1}{2}}) \\ &\quad - \frac{\Delta t}{\epsilon \Delta y} (H_{x,i,j+1,h}^{n+\frac{1}{2}} - H_{x,i,j,h}^{n+\frac{1}{2}}). \end{aligned} \quad (3)$$

The other five finite-difference equations can be obtained similarly [3].

Due to inherent numerical dispersive effects [4], the cell size is chosen to be as small as possible. Typically, the cell size should be less than  $\lambda_h / 10$ , where  $\lambda_h$  is the wavelength of the corresponding highest frequency of the excitation in the most optically dense medium. In order to obtain higher accuracy while maintaining acceptable memory requirements and running time, the cell size chosen for the studies presented herein is less than  $\lambda_h / 20$ . The time step is determined by the Courant-Friedrich-Lewy (CFL) stability criterion

$$\Delta t \leq \frac{1}{v_{max}} \left( \frac{1}{\Delta x^2} + \frac{1}{\Delta y^2} + \frac{1}{\Delta z^2} \right)^{-1/2}, \quad (4)$$

where  $v_{max}$  is the maximum phase velocity in the medium (typically, the free-space phase velocity).

Uniform plane-wave scattering from slots in finite and infinite conducting geometries are of interested in this study. The incident plane-wave source at infinity must be introduced into the algorithm without interfering with the scattered field. Several methods for implementing an incident plane-wave in the FDTD method have been previously given [4]. However, the choice of the source condition together with an ABC may lead to inaccurate results, and even impact the stability of the FDTD method.

The computational domain must be truncated with absorbing boundary conditions (ABCs). While several ABCs

have been proposed during the last decade, two ABCs were used in this study – second-order Mur [5] and Liao ABCs [6]. A second-order Mur is among the most frequently cited ABCs and, it works well in many cases. However, when the scatterer is too close to the absorbing boundaries as in the case of modeling a large or infinite conducting plane, instabilities may result. For one of the cases in this investigation, it was necessary to place the absorbing boundaries close to the scatterer because of limited computational resources. Liao ABCs were found to work better than Mur ABCs in this situation. Due to the inherent instability, Liao ABCs were used with double-precision arithmetic, although memory requirements were significantly increased. A modified form of Liao ABCs requires only single-precision arithmetic [7] but was found to be machine-dependent and not employed here.

### 3 Thin-Slot Subcellular Algorithms

The two subcellular thin-slot algorithms that are employed for modeling slots in enclosures and conducting plates are briefly discussed in this section. The first method introduced by Gilbert and Holland [1], denoted herein as the Capacitive Thin-Slot Formalism (C-TSF), is based on a simple and straight-forward quasi-static approximation. The second method, introduced by Riley and Turner [2], is a hybrid MOM/FDTD algorithm (HTSA).

Two-dimensional C-TSF results for plane-wave scattering from a slot in an infinite conducting plane have been shown to agree well with MOM results. Typical discrepancies of less than 10% can be expected for the field quantities at the locations near but not in the slot region [8]. The Yee cells around a slot with its axis parallel to the  $\hat{z}$ -axis are shown in Figure 1. Employing a quasi-static approximation for very narrow slots, and assuming the field quantities vary slowly in the  $\hat{z}$ -direction, the slot can be viewed as a coplanar, parallel strip capacitor [1]. The slot is then modeled by modifying the relative permittivity and relative permeability in the FDTD algorithm. Defining two line integrals, one transversed to the slot, and the other across the slot, the finite-difference field updating equations can be obtained for the nodes inside the slot. An extra parameter appears in the finite-difference equation which is the ratio of the two line integrals, and is shown to be an effective permittivity for the slot. The relative permittivity in the slot is then written as [1]

$$\epsilon_r = \frac{1}{\epsilon_0} \frac{\Delta y}{\Delta x} \frac{Q}{V} = \frac{1}{\epsilon_0} \frac{\Delta y}{\Delta x} C. \quad (5)$$

The capacitance is evaluated within only one cell, and is denoted the in-cell capacitance. In order to maintain the free-space phase velocity through the slot  $c_0 = 1/\sqrt{\epsilon_r \mu_r \epsilon_0 \mu_0}$ , the relative permeability in the slot is given by  $\mu_r = 1/\epsilon_r$ . Then in FDTD computation, the fields inside the slot can be updated by modifying only the permittivity and permeability as

$$E_{y,i,j,h}^{n+1} = E_{y,i,j,h}^n + \frac{\Delta t}{\epsilon_r \epsilon_0 \Delta z} (H_{x,i,j,h}^{n+\frac{1}{2}} - H_{x,i,j,h-1}^{n+\frac{1}{2}})$$

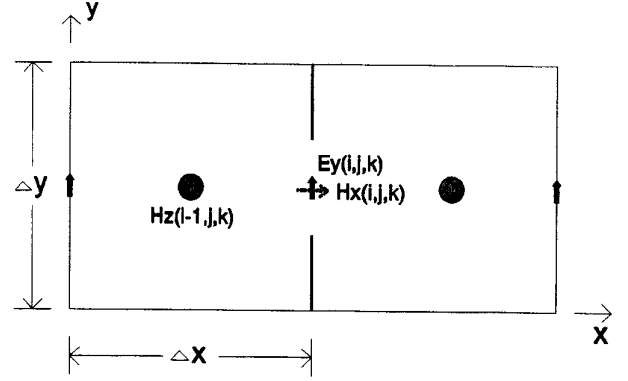


Figure 1: FDTD cells around the slot for the C-TSF subcellular algorithm.

$$H_{x,i,j,h}^{n+\frac{1}{2}} = H_{x,i,j,h}^{n-\frac{1}{2}} - \frac{\Delta t}{\epsilon_r \epsilon_0 \Delta x} (H_{x,i,j,h}^{n+\frac{1}{2}} - H_{x,i-1,j,h}^{n+\frac{1}{2}}) + \frac{\Delta t}{\mu_r \mu_0 \Delta z} (E_{y,i,j,h+1}^n - E_{y,i,j,h}^n) - \frac{\Delta t}{\mu_r \mu_0 \Delta y} (E_{x,i,j+1,h}^n - E_{x,i,j,h}^n), \quad (7)$$

for the slot shown in Figure 1.

A critical point is then determining the capacitance (or permittivity) to account for the slot. The capacitance of the slot can be found using the capacitance for a coplanar strip which is given analytically by [8]

$$C_{in-cell} = \frac{\epsilon_0 K \left[ \sqrt{1 - w_g^2 / \Delta y^2} \right]}{K(w_g / \Delta y)}, \quad (8)$$

or

$$\epsilon_r = \frac{K \left[ \sqrt{1 - w_g^2 / \Delta y^2} \right]}{K(w_g / \Delta y)}, \quad (9)$$

where  $K()$  is the complete elliptic integral of the first kind and  $w_g$  is the slot width. The integral equation based Hybrid Thin-Slot Algorithm (HTSA) is a sophisticated, and more complicated to implement thin-slot algorithm [2]. The HTSA is based on an integro-differential equation in the frequency domain developed for electromagnetic scattering from arbitrary slots and apertures in infinite conducting planes [9]. A section of a perfect electric conducting plate with a slot, embedded in Yee mesh is shown in Figure 2. An integro-differential equation for an equivalent problem is developed by shorting the plate and replacing the slot by an equivalent antenna with radius  $w_g/4$  for an infinitely thin plate. Then an integro-differential equation in time domain can be obtained as [2]

$$\mu_0 \frac{\partial (H_x^{sc2} - H_x^{sc1})}{\partial t} = 2 \left( \frac{\partial^2}{\partial x^2} - \frac{1}{c^2} \frac{\partial^2}{\partial t^2} \right) \int_{-L/2}^{L/2} \frac{K_x(x'; t - R_a/c)}{2\pi R_a} dx', \quad (10)$$

where

$$R_a = \sqrt{a^2 + (x - x')^2}, \quad (11)$$

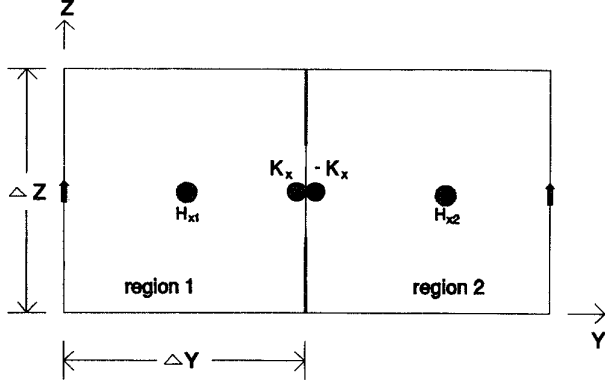


Figure 2: FDTD cells around the slot for the HTSA method. The plate is shorted. The electric fields inside the slot are set to zero, and replaced by equivalent magnetic currents on either side of the plane.

$H_x^{sc1,2}$  are the short-circuit fields in Regions 1 and 2, respectively and  $a$  is the equivalent antenna radius. The short-circuit magnetic field in Region 1 for example is the total field obtained in Region 1 as a result of an incident field scattering from the shorted plane. The total magnetic current  $K_x$  is  $K_x(x, t) = \int_{-w_g/2}^{w_g/2} dz M_x(z, x, t)$ ,  $\hat{x}M_x = \hat{y} \times \hat{z}E_a$ ,  $M_x$  is the magnetic current density, and  $E_a$  is the electric field in the aperture prior to shorting the conducting plane. This equation is derived based on image theory, and is strictly valid only for infinite planar PEC plates. By expanding the magnetic current with pulse basis functions in both space and time, then employing central differences for all differential operators, an explicit finite-difference equation for updating the magnetic current coefficients is obtained as

$$\begin{aligned}
K_i^n = & K_{i+1}^{n-1} + K_{i-1}^{n-1} - K_i^{n-2} \\
& + \frac{1}{2} \frac{\mu_0 \Delta^2}{\Delta t T_0} [(H_{x_1}^{n-1} - H_{x_1}^{n-2}) \\
& - (H_{x_2}^{n-1} - H_{x_2}^{n-2})] \\
& + \frac{1}{T_0} \sum_{i'=0, i \neq i'}^{N+1} [G_{|i-i'|}^a \\
& - (1 - \beta_{|i-i'|}) G_{|i-i'|}^{y_0}] \\
& [K_{i'+1}^{n-1-|i-i'|} + K_{i'-1}^{n-1-|i-i'|} \\
& - K_{i'}^{n-1-|i-i'|} - K_{i'}^{n-2-|i-i'|}] \\
& - \frac{1}{T_0} \sum_{i'=0}^{N+1} \beta_{|i-i'|} G_{|i-i'|}^{y_0} \\
& [K_{i'+1}^{n-2-|i-i'|} + K_{i'-1}^{n-2-|i-i'|} \\
& - K_{i'}^{n-1-|i-i'|} - K_{i'}^{n-3-|i-i'|}], \quad (12)
\end{aligned}$$

where

$$T_0 = G_0^a - (1 - \beta_0) G_0^{y_0} \quad (13)$$

$$G_\alpha^a = \frac{1}{2\pi} \ln \left[ \frac{(\alpha + \frac{1}{2})\Delta + \sqrt{[(\alpha + \frac{1}{2})^2 \Delta^2 + a^2]}}{(\alpha - \frac{1}{2})\Delta + \sqrt{[(\alpha - \frac{1}{2})^2 \Delta^2 + a^2]}} \right], \quad (14)$$

and  $\Delta$  is the cell size used in HTSA to discretize the slot, typically  $\Delta = \Delta x/2$  [2]. With a knowledge of the equivalent magnetic current, the slot can be accounted for by appending the magnetic current to the regular finite difference updating equation as

$$\begin{aligned}
H_{x_{1,2}}^{n+\frac{1}{2}} = & H_{x_{1,2}}^{n-\frac{1}{2}} - \frac{\Delta t}{\mu_0} (\nabla \times \bar{E}^n)_{x_{1,2}} \\
& \pm \frac{\Delta t}{\mu_0} \frac{1}{\Delta y} \frac{w_g}{\Delta z} \frac{1}{w_g} K_i^n, \quad (15)
\end{aligned}$$

where plus sign is for Region 2, and the minus sign is for Region 1. The HTSA can then be incorporated into the FDTD method in a straight-forward fashion by:

1. finding magnetic current coefficients using Equation (12) for time-step  $n$ ,
2. updating magnetic fields at time-step  $n + \frac{1}{2}$ ,
3. updating the magnetic current for the  $\bar{H}$ -field components adjacent to the slot as in Equation (15),
4. updating electric fields at time-step  $n + 1$ ,
5. reiterate until the late-time response is achieved.

In this fashion, the radiation from the magnetic current can be incorporated into the FDTD calculations. It should be noted that the  $\hat{z}$ -component of the electric field is set to zero, and the slot is completely accounted for in the FDTD algorithm by an equivalent magnetic current. This current affects the update equations for only those magnetic-field components parallel and adjacent (by one-half cell) to the slot as shown in Figure 2. One advantage of the HTSA over the C-TSF is the ability to model finite thickness slots through the equivalent current radius  $a$  [10].

## 4 Numerical Results

The C-TSF and HTSA subcellular algorithms were implemented with the FDTD method, and numerical results obtained for 3D finite plates, 3D loaded cavities, and a 3D infinite PEC plane with a finite-length slot. All the PEC walls are of vanishing thickness. Two excitations were used, a Gaussian pulse, and an electromagnetic pulse (EMP) [11]. Time-domain responses were converted to frequency-domain responses using a Fast Fourier Transform (FFT).

First, a thin slot in a finite plate was modeled in three dimensions. The dimensions of the plate and slot are shown in Figure 3. Both the C-TSF and HTSA methods were employed to model the slot. For the C-TSF, the relative permittivity is calculated using the coplanar strip capacitance formula [8] for the "in-cell" capacitance. For this case,  $\epsilon_r = 4.6141$  and  $\mu_r = 1/\epsilon_r$ . For the HTSA, the equivalent antenna radius is 0.001 cm. Cubic FDTD cells, 1 cm on a side, are used, and the total mesh dimensions are  $49 \times 49 \times 50$  in the  $\hat{x}$ ,  $\hat{y}$ , and  $\hat{z}$  directions, respectively. The plate was illuminated by a  $\hat{z}$ -directed TE (to the slot)

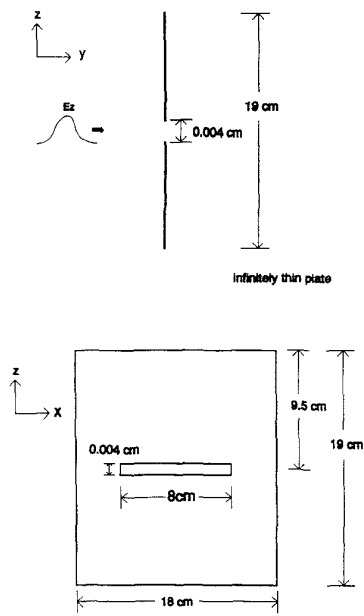


Figure 3: The geometry of the 3-D finite plate.

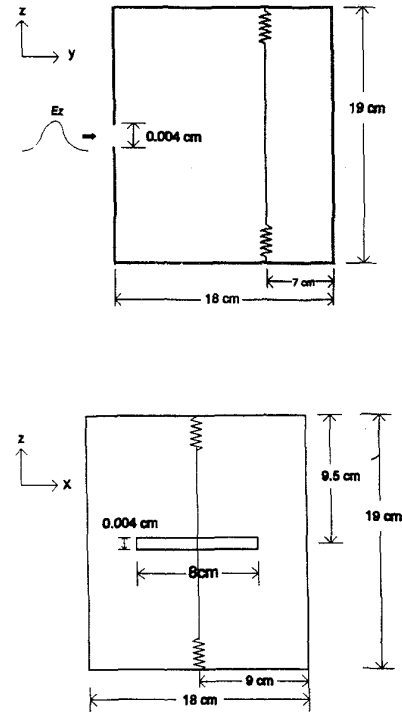


Figure 5: The geometry of the loaded cavity.

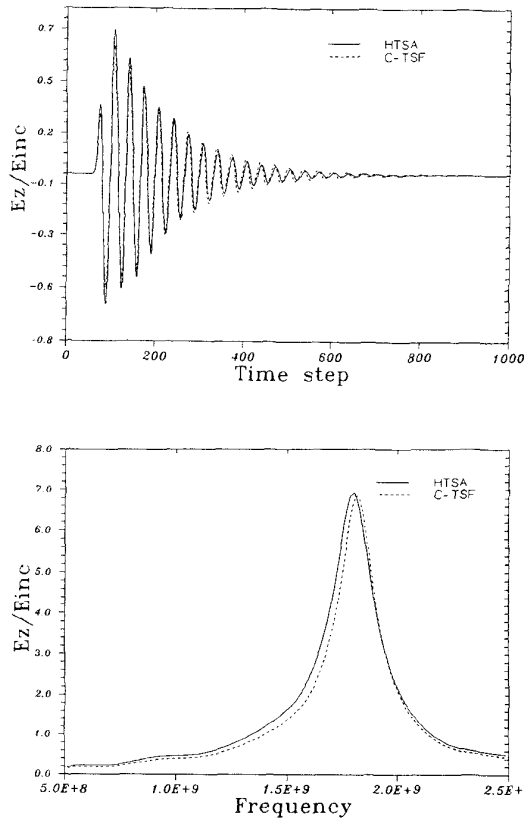


Figure 4:  $E_z$  sampled in the shadow region immediately adjacent to the slot. a) Time-domain results, and, b) FFT results

plane wave with a Gaussian-pulse temporal variation given by

$$E_z^{inc}(t) = e^{-\frac{(t-t_0)^2}{T^2}}, \quad (16)$$

where  $T = 1.214 \times 10^{-10}$ s and  $t_0 = 0.5 \times 10^{-9}$ s. The time step is 16.678 ps. The time delay is chosen to allow the pulse to start with approximately zero amplitude. A total-field/scattered-field formulation was used to implement the source. Second-order Mur ABCs are employed for surface boundary components, and first-order Mur ABCs for edge locations. Single-precision arithmetic is used for this case. The time-domain response for the  $z$  component of the electric field immediately adjacent to the slot for both the C-TSF and HTSA computations is shown in Figure 4(a). The comparison is in general good, however, there are small phase and amplitude differences. The corresponding frequency-domain response is shown in Figure 4(b).

A loaded rectangular cavity with a single slot is also modeled employing both the C-TSF and HTSA subcellular algorithms for the slot. The cavity dimensions are shown in Figure 5 [2]. All the relevant FDTD parameters for the mesh dimensions, computational domain, and excitation are the same as those employed for modeling the previous 3D plate. The cavity is loaded by a conducting wire with two  $50 \Omega$  resistors at both ends. The conducting wire is modeled using one cell by setting the tangential electric field along the wire axis to zero. The resistors are modeled with a subcellular algorithm reported in [12]. The current induced on the wire at the cavity center is calcu-

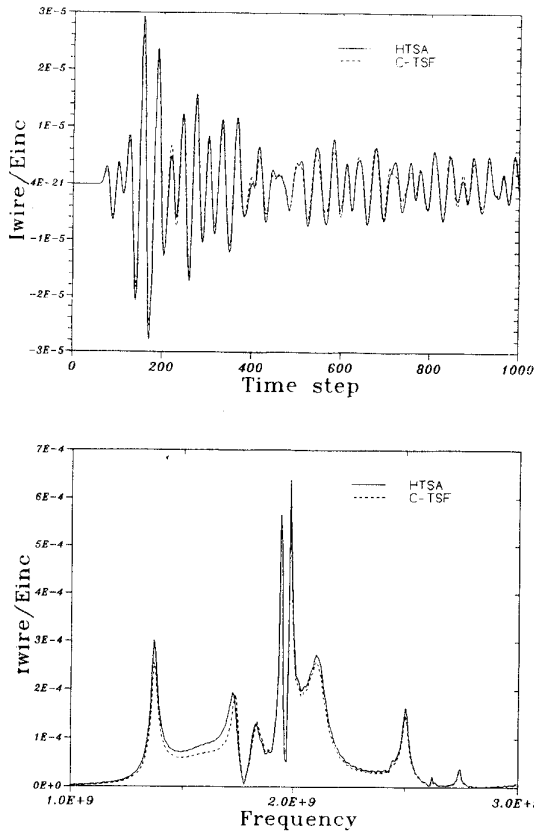


Figure 6: Time and frequency domain responses for the current induced on the wire in the loaded cavity.

lated from Ampere's law and is shown in Figure 6. The results again show good agreement between the two methods. While the resonance frequencies are nearly the same, there is some discrepancy in the amplitude over some frequency ranges. Scattering from a finite-length slot in a three-dimensional infinite PEC plane is also studied using the C-TSF and HTSA for modeling the slot. This problem is important because MOM, time-domain MOM, and experimental results are available in the literature for comparison [11]. The geometry of the plate, shown in Figure 7(a), is that employed by Reed and Butler [11]. Both C-TSF and HTSA are used to model the slot. The relative permittivity for the C-TSF method is  $\epsilon_r = 2.018$  corresponding to  $w_g = 1\text{mm}$ . A scattered field formulation and Liao ABCs are used. Double-precision arithmetic is used to avoid the inherent instability of the Liao ABCs. Since double-precision arithmetic is used, symmetry is exploited to reduce the memory requirements for the problem. Figure 7(b) shows the computational domain when symmetry conditions are applied. One symmetry plane and one truncation plane are chosen to reduce the computational domain to approximately 1/4 of the original size. Cubic FDTD cells, 0.5 cm on a side, are used, and the total mesh dimensions are  $36 \times 44 \times 23$  in the  $\hat{x}$ ,  $\hat{y}$ , and  $\hat{z}$  directions, respectively. The infinite PEC plane is illuminated by a  $\hat{z}$ -directed electromagnetic pulse of the form

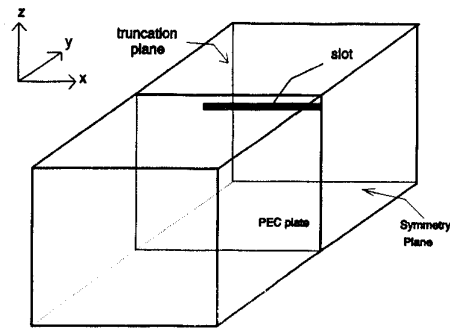
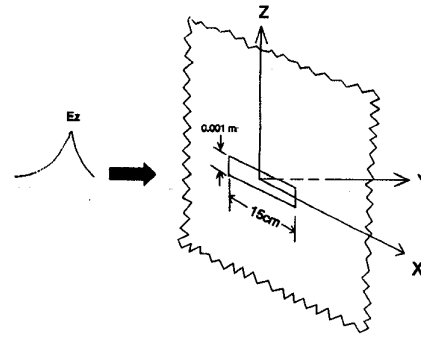


Figure 7: The geometry of the 3-D infinite conducting plane and the computational domain.

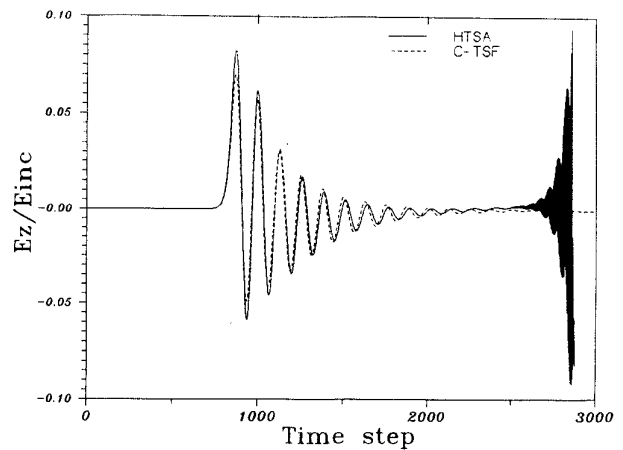


Figure 8: Time-domain responses of the slot excited by an EM pulse.

[11]

$$E_z^{inc}(t) = \frac{1}{0.8258} \frac{1}{e^{-20\frac{t-t_0}{\beta}} + e^{\frac{t-t_0}{\beta}}}, \quad (17)$$

where  $t_0 = 6.67 \times 10^{-9}\text{s}$  and  $\beta = 3.251 \times 10^{-9}\text{s}$ . The time step is 8.339 ps. For the HTSA, the equivalent antenna radius is 0.25 mm. Figure 8 shows the comparison of the time domain response for the C-TSF and HTSA methods.

$E_z$  at a point 5 cm away from the slot on the shadow side of the plane along the  $\hat{y}$ -axis is shown. Notice there is late-time instability occurring for HTSA method. By contrast, C-TSF is quite stable. In addition, preliminary results comparing C-TSF computations with experimental measurements show good agreement.

## References

- [1] J. Gilbert and R. Holland, "Implementation of the thin-slot formalism in the finite-difference EMP Code THREDII," *IEEE Trans. Nucl. Sci.*, vol. NS-28, no. 6, pp. 4269-4274, Dec. 1981.
- [2] D. J. Riley and C. D. Turner, "Hybrid thin-slot algorithm for the analysis of narrow apertures in finite-difference time-domain calculations," *IEEE Trans. Antennas Propagat.*, vol. AP-38, pp. 1943-1950, Dec. 1990.
- [3] D. M. Sheen, S. M. Ali, M. D. Abouzahra, and J. A. Kong, "Application of the three-dimensional finite-difference time-domain method to the analysis of planar microstrip circuits," *IEEE Trans. Microwave Theory Tech.*, vol. MTT-38, pp. 849-857, July 1990.
- [4] A. Taflove, notes, Northwestern University, 1992.
- [5] G. Mur, "Absorbing boundary conditions for the finite-difference approximation of the time-domain electromagnetic-field equations," *IEEE Trans. Electromagn. Compat.*, vol. EMC-23, pp. 377-382, Nov. 1981.
- [6] Z. P. Liao, H. L. Wong, B. P. Yang, and Y. F. Yuan, "A transmitting boundary for transient wave analysis," *Scientia Sinica*, vol. 27, no. 10, pp. 1063-1076, Oct. 1984.
- [7] M. Moghaddam, and W. C. Chew, "Stabilizing Liao's absorbing boundary conditions using single-precision arithmetic," in *Proc. 1991 IEEE AP-S Int. Symp., London, Ontario, Canada*, pp. 430-433, 1991.
- [8] C. D. Turner, and L. D. Bacon, "Evaluation of a thin-slot formalism for finite-difference time-domain electromagnetics codes," *IEEE Trans. Electromagn. Compat.*, vol. EMC-30, pp. 523-528, Nov. 1988.
- [9] C. M. Butler, Y. Rahmat-Samii, and R. Mittra, "Electromagnetic penetration through apertures in conducting surfaces," *IEEE Trans. Antennas Propagat.*, vol. AP-26, pp. 82-93, Jan. 1978.
- [10] C. A. Balanis, *Antenna Theory*, p. 338. John Wiley and Sons. 1982.
- [11] E. K. Reed, and C. M. Butler, "Time-domain electromagnetic penetration through arbitrarily shaped narrow slots in conducting screens," *IEEE Trans. Electromagn. Compat.*, vol. EMC-34, pp. 161-172, Aug. 1992.
- [12] Y. S. Tsuei, A. C. Cangellaris, J. L. Prince, "Rigorous electromagnetic modeling of chip-to-package (first-level) interconnections," *IEEE Trans. Comp., Hybrids., Manuf. Technol.*, vol. CHMT-16, pp. 876-883, Dec. 1993.